Materials Advances

ROYAL SOCIETY OF CHEMISTRY

PAPER

View Article Online
View Journal | View Issue

Cite this: *Mater. Adv.*, 2025, 6, 8414

Tumor matrix stiffness drives malignant progression in murine breast cancer: enhanced stemness, tumorigenesis and metastasis

Sadegh Safaei, †[abc] Samane Heydari, †[ab] Masoumeh Dehghan Manshadi,[ab] Behnaz Ashtari,[d] Mazaher Gholipourmalekabadi,[efg] Farhang Sasani,[h] Farideh Hashemi,[ab] Mehran Vosoogh,[i] Zahra Madjd*[ab] and Roya Ghods *[ab]

Matrix stiffness in the tumor microenvironment influences cancer cell behavior, including tumor growth and metastasis. We tested whether prior exposure to different stiffness levels creates a lasting mechanical memory that affects subsequent tumorigenesis and metastatic potential. We cultured 4T1 murine breast cancer cells on alginate–chitosan scaffolds mimicking normal (0.51 ± 0.13 kPa), fibrotic (3.40 ± 0.53 kPa), or tumoral (11.40 ± 0.96 kPa) breast tissue stiffness. We assessed cell morphology, proliferation, and expression of stemness markers (*Sox2*, *Nanog*, *Oct4*). After detachment, cells were injected into mouse mammary fat pads, and tumor latency, volume, and weight were monitored for 30 days. Lung and liver tissues were examined histologically for metastatic lesions and *Plac1* mRNA levels. Cells preconditioned on the stiff, tumor-mimicking scaffolds showed increased proliferation and stemness-marker expression *in vitro* and developed tumors with shorter latency, larger volume and weight, and more lung and liver metastases *in vivo*. These results indicate that a stiff matrix can imprint a persistent, pro-metastatic phenotype, consistent with a model of mechanical memory, enhancing tumorigenicity and metastatic spread. Targeting the mechanisms underlying this memory may offer new strategies to prevent breast cancer progression.

Received 23rd June 2025,
Accepted 7th October 2025

DOI: 10.1039/d5ma00664c

rsc.li/materials-advances

1. Introduction

The tumor microenvironment (TME), a complex and interactive ecosystem encompassing tumor cells and their surroundings, plays a pivotal role in cancer progression and metastasis.[1] Among its components, the extracellular matrix (ECM) not only provides structural support but also transmits biochemical and biophysical signals that critically influence cancer cell behavior.[2,3] One such biophysical property, matrix stiffness, defined as the resistance of the matrix to deformation,[4] is increasingly recognized as a key driver of tumorigenesis and metastasis. Clinically, elevated stiffness in mammary tissue correlates with a higher risk of breast cancer and increased disease aggressiveness.[5,6] Given the aggressive nature of triple-negative breast cancer (TNBC) and its poor prognosis,[7] understanding the role of mechanical memory in metastasis could reveal critical vulnerabilities for therapeutic intervention, potentially overcoming current limitations in treating metastatic disease, particularly in TNBC, which often exhibits resistance to conventional therapies. While this study focuses on TNBC, the findings may have relevance to other breast cancer subtypes where matrix stiffness plays a significant role.

[a] *Oncopathology Research Center, Iran University of Medical Sciences, Tehran, Iran. E-mail: ghods.ro@iums.ac.ir, rghods77@yahoo.com, majdjabari.z@iums.ac.ir, zahra.madjd@yahoo.com; Fax: +982188622608, +982188622608; Tel: +982186703212, +982186703212*
[b] *Department of Molecular Medicine, Faculty of Advanced Technologies in Medicine, Iran University of Medical Sciences, Tehran, Iran*
[c] *Monoclonal Antibody Research Center, Avicenna Research Institute, ACECR, Tehran, Iran*
[d] *Department of Medical Nanotechnology, Faculty of Advanced Technologies in Medicine, Iran University of Medical Sciences, Tehran, Iran*
[e] *Cellular and Molecular Research Center, Iran University of Medical Sciences, Tehran, Iran*
[f] *Department of Medical Biotechnology, Faculty of Allied Medicine, Iran University of Medical Sciences, Tehran, Iran*
[g] *Department of Tissue Engineering & Regenerative Medicine, Faculty of Advanced Technologies in Medicine, Iran University of Medical Sciences, Tehran, Iran*
[h] *Department of Pathology, Faculty of Veterinary Medicine, University of Tehran, Tehran, Iran*
[i] *Center of Experimental and Comparative Studies, Iran University of Medical Sciences, Tehran, Iran*
† Sadegh Safaei and Samane Heydari contributed equally to this manuscript as co-first authors.

Matrix stiffness increases through the accumulation, contraction, and crosslinking of ECM components by tumor cells and cancer-associated fibroblasts (CAFs).[8] This mechanical stiffness induces mechanical perturbations of the lipid bilayer and activates various ion channels and receptors, leading to cytoskeleton rearrangement and the activation of multiple downstream signaling pathways. These pathways promote the translocation of specific transcription regulators into the nucleus, regulating gene expression and subsequently affecting cellular fate, function, and characteristics.[9]

A pivotal characteristic of a distinct population of breast cancer cells within tumors is their stemness. These cells, known as cancer stem cells (CSCs), are a heterogeneous group of malignant cells characterized by their undifferentiated states and their ability to sustain long-term growth due to their self-renewal potential. CSCs play an important role in tumorigenesis and metastasis.[10] CSCs play an essential role at every stage of metastatic cell spread, undergoing epithelial–mesenchymal transition (EMT), inducing invasiveness,[11] and exhibiting cellular plasticity and dormancy.[12] The cellular plasticity of cancer cells is a primary cause of CSC-targeted therapy failure. Differentiated cancer cells can regenerate the CSC pool through microenvironmental cues, such as stiffness.[13] The stiffer matrix in invasive breast cancer cells can increase the proportion of cancer stem cell subpopulations.[14]

Investigating the effect of matrix stiffness on the invasion, migration, and metastasis of invasive breast cancer cells is a primary research focus. Several studies have evaluated the impact of increased stiffness on breast cancer cell phenotype, showing that higher stiffness can influence cell behavior, promote a more elongated cell shape, and enhance proliferation and invasiveness.[15]

Previous studies have found that high stiffness is important in inducing invasive phenotypes.[15–17] While some experiments attribute increased invasion to higher fiber content as an integrin ligand,[14,18] others show that, even when collagen density was constant, cells initially experienced inhibited invasion in stiffer environments but eventually adapted and became more invasive over time.[19] These observations among *in vitro* studies underscore the need for *in vivo* models to clarify matrix stiffness's precise role in tumor cell phenotype.

While the effects of stiffness on matrix-attached cells are increasingly understood, the role of persistent 'mechanical memory' in driving metastatic potential remains less explored. However, accumulating evidence suggests that these matrix-attached cells can retain a 'mechanical memory' of past mechanical experiences, influencing their long-term behavior. This phenomenon implies that cells exposed to a specific stiffness can maintain altered phenotypes, even after being transferred to environments with different mechanical properties.[20] This memory is thought to be mediated by various mechanisms, including persistent changes in cytoskeletal organization, epigenetic modifications, and alterations in gene expression.[21] These retained changes can significantly influence cell fate decisions, such as proliferation and stemness, and may play a crucial role in cancer progression and metastasis. Understanding the mechanical memory contribution to long-term cellular behavior in response to matrix stiffness is crucial for developing novel therapeutic strategies.[20]

By leveraging an *in vivo* model with chitosan–alginate scaffolds to isolate biophysical effects, this study directly addresses the mechanistic link between stiffness-induced memory and metastatic potential. We utilize 3D chitosan–alginate matrices designed to mimic the stiffness of normal (NBT), fibrotic (FBT), and tumoral breast tissue (TBT) (specific stiffness values will be detailed in the Methods section) to investigate their effects on the behavior of highly aggressive 4T1 cells. Chitosan–alginate scaffolds were selected for their tunable stiffness and ability to isolate stiffness properties from collagen biochemical properties, a key advantage over studies that relied on collagen gels with confounding variations in collagen biochemical properties. Using the 4T1 orthotopic implantation model, we examine how prior exposure to these varying stiffness levels influences subsequent tumor growth and spontaneous metastasis, focusing specifically on organ-specific colonization of the lungs and liver. Specifically, this study aims to: (1) characterize the effects of varying matrix stiffness on 4T1 cell proliferation and stemness *in vitro*; (2) determine whether prior exposure to different stiffness levels influences tumor growth and metastatic dissemination *in vivo*; and (3) investigate the role of mechanical memory in establishing distant metastases. These findings have the potential to provide insights into novel therapeutic strategies targeting mechanical memory to inhibit breast cancer metastasis and improve patient outcomes. Furthermore, these findings may have broader implications for understanding mechanotransduction in other cancers where matrix stiffness plays a significant role, such as pancreatic and liver cancer.

2. Materials & methods

2.1 Materials

In this study, alginic acid sodium salt (very low viscosity; CAS: 9005-38-3; Alfa Aesar) and low molecular weight chitosan (50 000–190 000 Da; CAS: 9012-76-4; Sigma Aldrich) were used. The reagents included Roswell Park Memorial Institute (RPMI)-1640 medium (Sigma Aldrich), fetal bovine serum (FBS) (Gibco), penicillin–streptomycin (Gibco), trypsin-EDTA (Bio Basic), dimethyl sulfoxide (DMSO) (Bio Basic), 3-(4,5-dimethylthiazol-2-yl)-2,5-diphenyltetrazolium bromide (MTT) (Sigma Aldrich), ketamine (Alfasan), and xylazine (Alfasan).

2.2 Evaluation of stiffness in normal and tumoral mouse breast tissues

To inform the design of our scaffolds, we evaluated the stiffness of murine breast tissue representative of normal and tumoral states. We measured the stiffness of murine adipose tissue, which serves as a model for normal breast tissue matrix,[22] and 4T1-induced murine breast tumors were harvested from female Balb/c mice following the induction of tumors. Fresh tissue samples were collected immediately prior to mechanical

testing. Uniaxial compressive tests were performed to evaluate the mechanical properties of tissue specimens. The tests were performed using a SANTAM Universal Testing Machine (STM-1; Iran), which is equipped with a 1000 N load cell capacity to accurately measure the applied compressive forces. A crosshead speed of 1 mm min^{-1} was applied during compression. The compressive modulus (kPa) was calculated from the slope of the initial linear portion of the stress–strain curve. The data are presented as mean ± standard deviation (SD).

Fibrotic breast tissue, in comparison with normal tissue, exhibits increased stiffness, which varies based on the extent of collagen.[5] However, we did not directly measure the stiffness of fibrotic breast tissue in this study. Instead, we considered the stiffness of fibrotic tissue based on the values reported by Paszek *et al.*,[23] who demonstrated a range of stiffnesses in the tumor-attached stroma. The specific value used to represent fibrotic tissue in our *in vitro* scaffolds was determined based on the relative stiffnesses we measured for normal adipose tissue and 4T1-induced tumors and will be detailed in the Results section.

2.3 Preparation of alginate–chitosan scaffolds

Scaffolds mimicking the stiffness of normal, fibrotic, and tumoral mouse breast tissues (NBT, FBT, and TBT scaffolds, respectively) were prepared following a basic method similar to previously reported techniques,[24] with specific modifications in chitosan and alginate concentrations to achieve distinct stiffnesses relevant to breast tissue environments. In detail, they were developed using three different combinations of chitosan and alginate concentrations. To make the chitosan solution, chitosan powders were dissolved in acetic acid solution (2% v/v) at concentrations of 1%, 2, and 4% (w/v). These mixtures were constantly stirred for over one hour until uniform solutions were formed. Subsequently, corresponding alginate solutions at concentrations of 1%, 2%, and 4% (w/v) were prepared by dissolving alginate in deionized water. The 1% alginate solution was added to the 1% chitosan solution, the 2% alginate solution was added to the 2% chitosan solution, and the 4% alginate solution was added to the 4% chitosan solution. Following pH adjustment to 4.7, the resulting mixtures were stirred for over two hours to achieve homogeneous chitosan–alginate (Alg/Chi) solutions.

Each solution was poured into 24-well cell culture plates and frozen at −20 °C for 12 hours. The samples were then lyophilized, sectioned, crosslinked in a 0.2 M $CaCl_2$ solution for 15 minutes, washed several times with deionized water to remove any excess salt, and sterilized in 70% ethanol for 1 hour. The scaffolds were finally transferred to a sterile PBS solution (pH = 7.4) to remove any remaining ethanol.[25] These scaffolds were designed to vary in stiffness corresponding to the stiffness of murine normal, fibrotic, and tumoral breast tissues.

2.4 Evaluation of scaffolds stiffness

The stiffness of the hydrated scaffolds that had been prepared was determined using the methods outlined in Section 2.2.

2.5 Morphological and pore size analysis by scanning electron microscopy (SEM)

The surface morphology and pore size of the different types of scaffolds (n = 3 per group) were studied by SEM. The scaffolds had undergone lyophilization during the initial fabrication process. Prepared samples were subsequently coated with gold–palladium for conductivity. The SEM imaging was performed on these dry scaffolds (Seron Technology, AIS-2100, Korea) to visualize their porous structure and morphology.

The average pore size of each scaffold composition was calculated from representative SEM images using ImageJ software (**https://imagej.net/software/imagej/**). To quantify the average pore size, measurements were obtained from multiple pores across 20 distinct locations per dry sample (n = 3 per group), with an average of 17 pores measured per location. These measurements resulted in pore size values reported in μm.

2.6 Measurement of swelling degree

The water absorption capacity of the scaffolds was determined through a swelling test. To do this, each group of scaffolds (n = 3) was weighed in the dry state and then immersed in PBS (pH = 7.4) at 37 °C for varying amounts of time (1, 2, 4, 6, and 24 hours). After removing the excess surface water with filter paper, the scaffolds were weighed again. Using eqn (1), where W_w is the weight of the swollen scaffold, and W_d is the initial dried weight, the swelling ratio was then calculated:

$$\text{Swelling (\%)} = (W_w - W_d)/W_d \times 100 \quad (1)$$

2.7 Measurement of porosity

The liquid displacement process was used to determine the porosity of scaffolds.[26] For each scaffold group, three samples were prepared. Each sample was individually placed in a graduated beaker filled with a known volume (V_1) of absolute ethanol due to its ability to penetrate into the pores easily without causing significant shrinkage or swelling of the scaffold material.[22] The samples were incubated at 25 °C for 24 hours in a vacuum oven to allow the ethanol to penetrate the pores. The sum volume of both ethanol and scaffold was then recorded as V_2. After the scaffold was removed from the beaker, the remaining ethanol volume was noted down as V_3. Finally, by using eqn (2), the porosity of the scaffold (ε) was calculated as follows:

$$\varepsilon\ (\%) = ((V_1 - V_3)/(V_2 - V_3)) \times 100 \quad (2)$$

2.8 Evaluation of hydrolytic degradation

For each scaffold group, three samples were prepared. Each sample was individually put into 3 ml of PBS (pH = 7.4) and incubated at 37 °C for each interval (1, 3, and 7 days). After the defined time, the scaffolds were freeze-dried for 12 hours before weighing, to ensure accurate and consistent measurement of the dry mass of the scaffold, free from any residual water. Ultimately, using eqn (3), the percentage of weight loss

was calculated by taking into account the initial dry mass (M_0) and the terminal dry mass (M_1) of the scaffolds.[27]

$$\text{Weight loss (\%)} = ((M_0 - M_1)/M_0) \times 100 \quad (3)$$

2.9 Fourier-transform infrared (FTIR) analysis

To determine the chemical composition and the bonds formed between different components of prepared scaffolds, FTIR spectra were recorded for scaffolds and also pure alginate and chitosan powder, as controls. The samples (n = 3) were pelletized with potassium bromide (KBr) powder and analyzed using a PerkinElmer Spectrum Two FTIR spectrometer (PerkinElmer, USA). The spectra were acquired in transmittance mode with a resolution of 4 cm^{-1} and over a wavenumber range of 400–4000 cm^{-1} with a scan speed of 16 scans per spectrum.

2.10 Cell culture

The highly metastatic mouse mammary adenocarcinoma cell line, 4T1, was acquired from the National Cell Bank of Iran (Pasteur Institute of Iran, Tehran, Iran). The cells were maintained in RPMI-1640 medium, supplemented with 10% FBS, 100 U mL^{-1} penicillin, and 100 mg L^{-1} streptomycin. They were kept in a humidified atmosphere of 5% CO_2 at 37 °C and passaged in T-25 cell culture flasks at 90% confluency. Seeding of cells on the scaffolds was done by harvesting them after two passages using 2.5 g L^{-1} porcine trypsin and 0.2 g L^{-1} EDTA for 3 minutes at 37 °C, followed by inactivation with complete media and centrifugation at 300 × g for 3 minutes to form cell pellets. The cells were suspended in fully supplemented media and seeded onto three groups of 3D chitosan–alginate scaffolds in 24- or 48-well plates. In 3D culture, cell adhesion was allowed for 1.5 hours before adding media, and the scaffolds were transferred to new well plates after 6 hours to avoid any effects from cells attached to the bottom of the wells. All samples were cultured for seven days in a humidified incubator at 37 °C with 5% CO_2, and the media was changed every other day.

2.11 Evaluation of seeding cells attachment and morphology

To study the attachment and morphology of 4T1 cells on prepared scaffolds, 50 000 cells were seeded on a 24-well plate with NBT, FBT, or TBT scaffolds. After three days of incubation, cell-seeded scaffolds were fixed using 2.5% glutaraldehyde in PBS (pH = 7.4) for 30 minutes. Subsequently, samples were dehydrated using a graded ethanol series (50, 60, 70, 80, 90, and 100% for 5 minutes each). Specimens were then coated with gold–palladium and examined using SEM (Seron Technology, AIS-2100, Korea). The obtained SEM images were analyzed as described in Section 2.5.

2.12 Assessment of seeding cell viability by MTT assay

MTT assays were performed to assess the effect of NBT, FBT, and TBT scaffolds on the viability of 4T1 seeding cells. The 48-well plates were used to seed 5000 cells per scaffold, which were then incubated for 1, 3, and 7 days in a humidified incubator at 37 °C with 5% CO_2. The culture medium was replaced with a fresh medium every other day. The experimental design involved seven groups with three replicates for each time interval. Three groups included seeding cells on NBT, FBT, and TBT scaffolds, all three scaffolds without cells and wells without scaffolds served as negative controls. At each time point, the media was replaced with 200 µl of culture media containing 0.5 mg ml^{-1} MTT and incubated for 3 hours in the dark, at 37 °C with 5% CO_2. The insoluble formazan produced by the mitochondria of living cells was dissolved in DMSO. After 20 minutes of shaking at 37 °C and in dark condition, 100 µl of the dissolved formazan dye in each well was transferred to a new 96-well plate. The absorbance of formazan was measured at 570 nm, while a reference wavelength was 630 nm. The resulting data was the mean ± SD.

2.13 Assessment of stemness related gene expression

The stiffness-mediated changes in stemness-regulating genes in 4T1 cells, such as SRY-Box Transcription Factor 2 (*Sox2*), Nanog Homeobox (*Nanog*), and octamer-binding transcription factor 4 (*Oct4*), were analyzed. Total RNA was extracted from 4T1 cells that were seeded and cultured onto NBT, FBT, and TBT scaffolds in 24-well plates for seven days (n = 3), using One Step-RNA Reagent (Bio Basic, BS410A, Canada), according to the manufacturer's instructions. The complementary DNA was synthesized with the Yekta Tajhiz Azma cDNA Synthesis Kit (YT4500; Tehran, Iran), and then Quantitative PCR amplification was performed by qPCR kit (Ampliqon A325402-25 2x qPCR Master mix green-High Rox) using PCR Cycler Light Q Gene-R (Qiagen, Germany). The reaction was preheated at 95 °C for 15 min, followed by 40 cycles of 95 °C for 15 s, 60 °C for 15 s, and 72 °C for 15 s; PCR products were validated using melting curve analysis. Relative expression levels were calculated compared to *Gapdh* expression levels. Primers used for PCR were *Oct4*: forward, 5′-GTTCTCTTTGGAAAGGTGTTC-3′; reverse, 5′-GCATATCTCCTGAAGGTTCTC-3′. *Nanog*: forward, 5′-TGATTTGGTTGGTGTCTTG-3′; reverse, 5′-TGTGATGGCGAGGGAAG-3′. *Sox2*: forward, 5′-AAAGGGTTCTTGCTGGGTTT-3′; reverse, 5′-AGACCACGAAAACGGTCTTG-3′. *Gapdh*: forward, 5′-AACTTTGGCATTGTGGAAGG-3′; reverse, 5′-CACATTGGGGGTAGGAACAC-3′.

2.14 Animals

All animal experiments were performed following the guidelines of the animal research committee of Iran University of Medical Sciences (IUMS) and approved by the Ethics Committee for Animal Experiments (No. IR.IUMS.REC 1396.32781). This study also adheres to the principles outlined in the EU Directive 2010/63 for the protection of animals used for scientific purposes. Female Balb/c mice, aged 6–8 weeks, were obtained from the Pasteur Institute of Iran (Alborz, Iran). Upon arrival, mice were allowed to acclimatize for seven days before the commencement of any experimental procedures. Animals were housed under controlled environmental conditions: temperature (25 ± 2 °C), humidity (50 ± 5%), and a 12-hour light/dark cycle. Food and water were provided *ad libitum*. The sample size for animal assays was determined in accordance with the ARRIVE 2.0 guidelines to adhere to the principle of reduction, ensuring the ethical use of

animals in a resource-limited setting. The findings are interpreted primarily as biologically relevant trends.[28]

2.15 *In vivo* experimental design

Mice were randomly assigned to three experimental groups (n = 3 per group): (1) NBT-preconditioned cells, (2) FBT-preconditioned cells, and (3) TBT-preconditioned cells. Randomization was performed using a random number generator after the mice were assigned a unique identification number. In the *in vivo* approach, 50 000 4T1 cells were seeded and cultured on NBT, FBT, and TBT scaffolds for seven days, as described before. Following this preconditioning period on the biomimetic scaffolds, the adherent cells were detached using a standard enzymatic method, trypsin-EDTA. The detached cells were then collected, counted, and re-suspended in sterile PBS (pH = 7.4) and injected at a number of 100 000 cells per animal directly into the right side inguinal mammary fat pads of mice. Moreover, a control group that did not receive any cancer cells was included.

2.16 Assessment of tumor formation and volume

The tumorigenesis was monitored through three methods. Firstly, the day a palpable tumor appeared in each mouse was recorded. Secondly, once the tumor appeared, its volume was measured every two days using calipers. The investigator performing the palpations and tumor volume measurements was blinded to the group allocations. On the day that tumor volume in one of the mice reached 1800 mm^3, all animals were humanely sacrificed, tumors were excised, and tumor weight was measured.

2.17 Measurement of metastasis

2.17.1 Histology analysis. Before sacrificing the animals, mice were anesthetized. The lung and liver, as the main target organs for breast cancer metastasis, were harvested. To examine any pathological changes, half of the harvested tissue was fixed in a 10% formalin solution, followed by paraffin embedding for hematoxylin and eosin (H&E) staining.

H&E-stained sections were visualized by veterinary pathology specialist who was blinded to the group assignments using an optical microscope (Olympus BX51) equipped with a high-resolution camera (Olympus DP71). The mitotic index (MI) was determined by counting the number of mitotic figures (cells undergoing division) within ten randomly selected high-power fields (HPF) at 400× magnification for each sample. The average number of mitotic figures per HPF was then calculated. This allowed for the comparison of proliferative activity across different groups.

The quantitative assessment of metastasis was performed by counting metastatic nodules and calculating metastatic areas in ten randomly selected microscopic fields per organ for each group. Nodules were counted by a blinded, accredited pathologist using a microscope with a 10× objective. In accordance with established methods[29,30] metastatic areas were measured using ImageJ software; tumor regions were delineated, and their surface areas were calculated, excluding immune cells such as neutrophils.

2.17.2 Placenta-specific 1 (*Plac1*) expression as a representative of 4T1 cells. *Plac1* is a member of cancer-testis antigens that are expressed by a variety of human and murine cell lines,[31] including 4T1.[32] However, normal cells of mature female mice do not express it except for the brain cerebellum.[33] Therefore, in the present study, the *Plac1* expression as a representative of 4T1 cells was investigated in the whole lung and liver of mice (two common target organs for 4T1 metastasis) (ref. 32). So, the other half of the harvested tissue was utilized to detect the *Plac1* transcripts using real-time PCR, by the method that was previously described. The reaction was preheated at 95 °C for 15 min, followed by 45 cycles of 95 °C for 15 s, 62 °C for 15 s, and 72 °C for 15 s; PCR products were validated using melting curve analysis. Relative expression levels were calculated compared to *Gapdh* expression levels. Primers used for PCR were *Plac1*: forward, 5′-AGGAGAATC CTTCCTGGACG-3′; reverse, 5′-GTCGAGCACAGCACATTCAC-3′. *Gapdh*: forward, 5′-AACTTTGGCATTGTGGAAGG-3′; reverse, 5′-CACATTGGGGGTAGGAACAC-3′.

2.18 Data analysis

Experimental data were analyzed with the GraphPad Prism 8.4.3 software. The unpaired t-test was employed to compare stiffness, average pore size, porosity, tumor weight, and latency of tumor detection between each two groups. Additionally, a one-way ANOVA analysis was conducted to compare gene expression levels. For assessing tumor volumes over time, we utilized a paired t-test. Furthermore, the swelling degree, hydrolytic degradation degree, and absorbance in the MTT assay were subjected to two-way ANOVA. All data are presented as mean ± SD and statistical significance was determined using a threshold of $P < 0.05$.

3. Results

3.1 Alginate–chitosan scaffolds appearance and stiffness

Alginate–chitosan scaffolds were prepared with varying concentrations of chitosan and alginate solutions to mimic the stiffness of normal, fibrotic, and tumoral mouse breast tissues. Specifically, for the NBT scaffold, a 1 wt% chitosan solution and a 1 wt% alginate solution, for the FBT scaffold, a 2 wt% chitosan solution, and a 2 wt% alginate solution, and for the TBT scaffold, a 4 wt% chitosan solution and a 4 wt% alginate solution were used. The final appearance of the dry alginate–chitosan scaffolds is shown (Fig. 1(a)). The mean stiffness (compressive moduli) of murine adipose tissue and each scaffold in the wet state was obtained from the initial linear slope of the stress–strain curve and reported in Fig. 1(b).

Murine adipose tissue, closely resembling normal breast tissue, exhibited a stiffness of 0.39 ± 0.04 kPa. 4T1-induced tumors exhibited a stiffness of 10.5 ± 2.9 kPa, consistent with reported values of 9.09 ± 3.2 kPa for murine tumoral breast tissue.[34] The stiffness of fibrotic breast tissue is known to vary with collagen content but generally falls between normal and

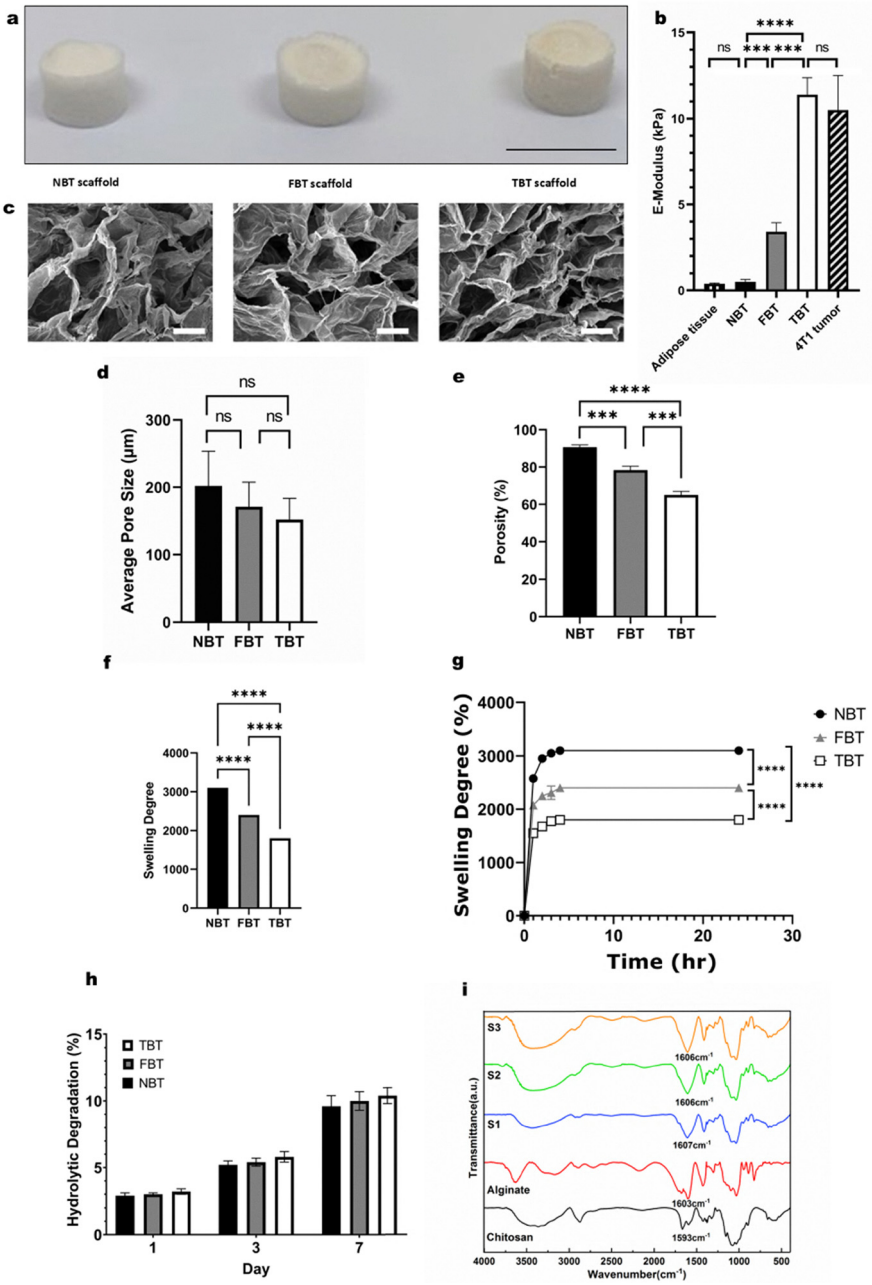

Fig. 1 Characterization of alginate–chitosan scaffolds. (a) Macroscopic appearance. Representative photographs of normal breast tissue-mimicking (NBT; 1 wt% chitosan, 1 wt% alginate), fibrotic breast tissue-mimicking (FBT; 2 wt% chitosan, 2 wt% alginate), and tumoral breast tissue-mimicking (TBT; 4 wt% chitosan, 4 wt% alginate) scaffold discs in the dry state. Scale bar = 10 mm. (b) Compressive modulus (stiffness). Mean compressive moduli of NBT, FBT, and TBT scaffolds, compared to murine tumoral and adipose tissue. (c) Pore morphology. Representative scanning electron microscopy (SEM) images showing the pore structure of NBT, FBT, and TBT scaffolds. Scale bar = 100 μm. (d) Average Pore Size. Quantification of average pore size in NBT, FBT, and TBT scaffolds. (e) Porosity. Measured porosity of NBT, FBT, and TBT scaffolds. (f) Maximum swelling degree. Maximum swelling degree of NBT, FBT, and TBT scaffolds after 6 hours in PBS (pH = 7.4). (g) Swelling Kinetics. Swelling behavior of NBT, FBT, and TBT scaffolds over time (1, 2, 4, 6, and 24 hours) in PBS (pH = 7.4). (h) Hydrolytic degradation. Hydrolytic degradation of NBT, FBT, and TBT scaffolds after 1, 3, and 7 days in PBS at 37 °C. (i) Fourier transform infrared spectroscopy (FTIR) analysis. FTIR spectra of NBT, FBT, and TBT scaffolds, confirming polyelectrolyte complex formation between alginate and chitosan. The peak at 1607 cm^{-1} confirms complex formation, resulting from the combination of the amide I chitosan peak (1666 cm^{-1}) and the COO^- asymmetric alginate peak (1603 cm^{-1}). Data are expressed as mean ± SD (n = 3). Statistical significance is indicated as follows: *$p < 0.05$, **$p < 0.01$, ***$p < 0.001$, and ****$p < 0.0001$.

tumoral values.[23] To mimic this, we fabricated an FBT scaffold (2 wt% chitosan, 2 wt% alginate) with a stiffness of 3.40 ± 0.53 kPa. This value is intermediate between the measured stiffnesses of the NBT scaffold (0.51 ± 0.13 kPa, mimicking normal adipose tissue) and the TBT scaffold (11.40 ± 0.96 kPa, mimicking tumoral tissue) and was chosen based on relative stiffness values reported by

Paszek *et al.*[23] The stiffnesses of the NBT, FBT, and TBT scaffolds were significantly different ($p < 0.05$).

3.2 Average pore size and percent porosity of scaffolds

Average pore size and porosity were assessed to ensure that the scaffolds are appropriate for cell infiltration and growth and to compare how different concentrations of alginate–chitosan affect these variables. Based on the SEM images, all scaffolds were porous with interconnected pore structures and random orientation (Fig. 1(c)). The average pore size in the dry scaffolds were 202 ± 40 μm, 171 ± 33 μm, and 152 ± 38 μm, for NBT, FBT, and TBT scaffolds, respectively (Fig. 1(d)). The results indicate that there was no significant difference in pore size between the scaffolds. The NBT, FBT, and TBT scaffolds had 90.67 ± 1.1%, 78.33 ± 2.1%, and 65.00 ± 2.0% porosities, respectively (Fig. 1(e)), which indicate scaffolds had a statistically significant difference ($p < 0.001$) in porosity compared with each other.

3.3 Swelling degree of scaffolds

To determine prepared scaffolds' capacity to swell and retain fluids, ensuring they possess sufficient qualities for nutrient transport and mechanical stability, and to compare how different concentrations of alginate–chitosan affect these properties, the swelling degree of scaffolds was assessed. The maximum swelling degree obtained after 6 hours for NBT, FBT, and TBT scaffolds can be observed in Fig. 1(f), which were 3100 ± 0%, 2400 ± 0%, and 1800 ± 0%, respectively, and were significantly different ($p < 0.0001$) with each other. The NBT scaffolds exhibited the highest swelling percentage. As shown in Fig. 1(g), the swelling percentage decreases with increasing concentrations of alginate and chitosan, particularly in the TBT scaffolds, which had the lowest values. Furthermore, to observe how the scaffold properties change over time and ensure they maintain their functionality for nutrient transport and mechanical stability, the swelling behavior of each scaffold over time is shown in Table 1.

3.4 Hydrolytic degradation of scaffolds

Hydrolytic degradation analysis was performed on the three groups of scaffolds after 1, 3, and 7 days (Table 2 and Fig. 1(h)) to determine the longevity and stability of scaffolds. No significant differences were observed in the degradation rates among the three scaffolds.

Table 1 Swelling of NBT, FBT, and TBT scaffolds as a function of time (1, 2, 4, 6, and 24 hours, $n = 3$)

Time (hour)	NBT (% swelling)	FBT (% swelling)	TBT (% swelling)
1 hour	2575 ± 35	2075 ± 35	1550 ± 71
2 hours	2950 ± 71	2250 ± 70	1675 ± 35
4 hours	3050 ± 71	2310 ± 127	1775 ± 35
6 hours	3100 ± 0	2400 ± 0	1800 ± 0
24 hours	3100 ± 0	2400 ± 0	1800 ± 0

Data are expressed as mean ± SD.

Table 2 Hydrolytic degradation of NBT, FBT, and TBT scaffolds over 1, 3, and 7 days ($n = 3$)

Scaffold type	1 Day (% degradation)	3 Days (% degradation)	7 Days (% degradation)
NBT	2.9 ± 0.2	5.2 ± 0.3	9.6 ± 0.8
FBT	3.0 ± 0.1	5.4 ± 0.3	10.0 ± 0.7
TBT	3.2 ± 0.2	5.8 ± 0.4	10.4 ± 0.5

Data are expressed as mean ± SD.

3.5 FTIR analysis

During the preparation of alginate–chitosan scaffolds, cationic chitosan can form polyelectrolyte complexes with alginate, an anionic polymer, through electrostatic interactions. The formation of these complexes in the NBT, FBT, and TBT scaffolds was evaluated using FTIR analysis and presented in Fig. 1(i). The characteristic peaks in the alginate spectra include the peaks at 1603 cm^{-1} (COO^- asymmetric stretch), 2889 cm^{-1} (C–H stretch), and 3629 cm^{-1} (O–H stretch). The characteristic peaks in the chitosan spectra include the peaks at 2875 cm^{-1} (C–H stretch), 1666 cm^{-1} (amide I), and 1593 cm^{-1} (amide II). Alginate–chitosan polyelectrolyte complex formation is confirmed by the combination of amide I (1666 cm^{-1}) and N–H bending of amide II (1593 cm^{-1}) chitosan peaks and the COO^- asymmetric (1603 cm^{-1}) alginate peak into one peak at 1607 cm^{-1}, which is shown on the NBT, FBT, and TBT scaffolds spectra.

3.6 Attachment and morphology of the 4T1 cells on the scaffolds

Three days after the seeding of 4T1 cells on alginate–chitosan scaffolds mimicking NBT, FBT, and TBT stiffness, their attachment and morphology were investigated using SEM imaging. As shown in Fig. 2, 4T1 cells were well attached to all three scaffolds. On the NBT scaffold, several single cells with rounded morphology and flattened cell aggregations were observed. In contrast, on the TBT scaffold, the number of single round cells was decreased; instead, cells with several elongated filopodia and stellate shapes appeared. Moreover, cell aggregations with irregular shapes were detected, which were smaller and more spherical on top and stellate form at the surface contact area. Cells cultured on the FBT scaffold showed intermediate characteristics between the NBT and TBT groups. In images of this group, a few rounded single cells and various-sized aggregations with spherical shapes were observed. These findings indicate that scaffold stiffness significantly influences 4T1 cell morphology and aggregation patterns.

3.7 Cell viability assay of the cultured 4T1 cells on the scaffolds

An MTT assay was performed to assess the impact of matrix stiffness on 4T1 cell viability. 4T1 cells were cultured on NBT, FBT, and TBT scaffolds, and their viability were measured at 1-, 3-, and 7 days post-seeding (Fig. 3(a)). While all three scaffolds supported cell viability over time, TBT scaffolds

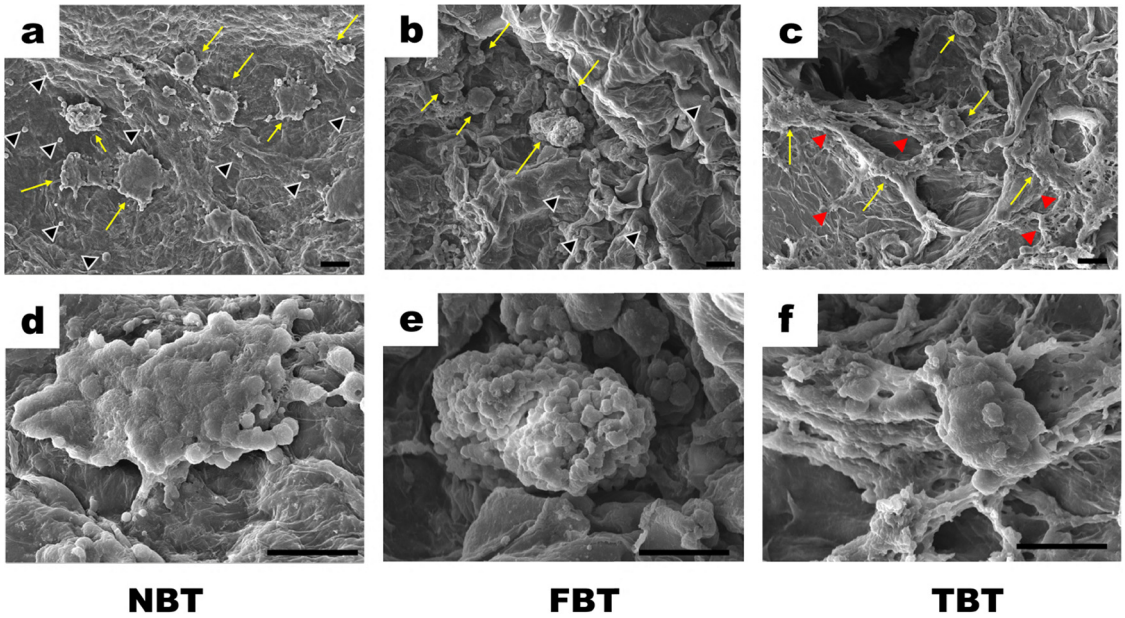

Fig. 2 4T1 cell morphology on scaffolds of varying stiffness. Scanning electron microscopy (SEM) images of 4T1 cells cultured for 3 days on scaffolds mimicking normal breast tissue (NBT; a, d), fibrotic breast tissue (FBT; b, e), and tumoral breast tissue (TBT; c, f). Magnifications: 500× (a, b, c) and 2000× (d, e, f). Yellow arrows indicate cell aggregations, black arrowheads indicate single cells, and red arrowheads indicate cell filopodia. Scale bar = 30 μm.

demonstrated the higher value relative to NBT, significantly at day 7, indicating superior cell viability on this matrix.

3.8 Stemness-related gene expression of cultured 4T1 cells on scaffolds

Real-time PCR was performed to assess the effect of varying stiffness scaffolds on the expression of stemness-related genes of *Sox2*, *Nanog*, and *Oct4* in 4T1 cells cultured on NBT, FBT, and TBT scaffolds for seven days (Fig. 3(b)). In cells cultured on the TBT scaffold, the mRNA expression of these stemness-related genes was upregulated, and the upregulation was found to be significantly higher than the other two groups. Furthermore, the expression of these genes in 4T1 cells cultured on the FBT scaffold showed an increase compared to cells on the NBT scaffold, although this increase was not found to be statistically significant.

3.9 Tumorigenic potential of the cultured 4T1 cells on varying stiffness scaffolds

To investigate whether various matrix stiffnesses affect tumorigenesis in a murine model of breast cancer, and also, to evaluate the persistence of matrix stiffness effect in the memory of murine breast cancer cells, 4T1 cells cultured for seven days on NBT, FBT, and TBT scaffolds and then using trypsin-EDTA detached from them and individually injected into the right mammary fat pad of mice. Tumor latency, as defined by the days between tumor cell inoculation and palpable tumor detection, tumor volume over time, and tumor weight on day 30 post-injection of 4T1 cells were investigated in mice. As illustrated in

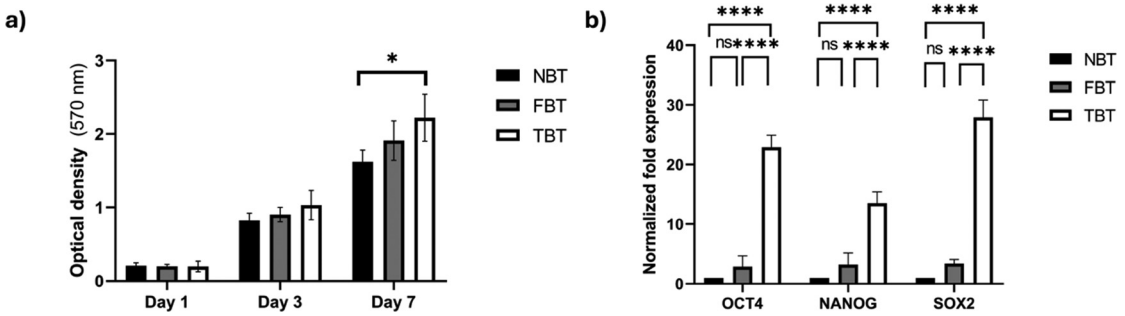

Fig. 3 Effect of matrix stiffness on 4T1 murine mammary carcinoma cell viability and stemness *in vitro*. (a) Cell viability. 4T1 cells were cultured on chitosan–alginate scaffolds mimicking normal breast tissue (NBT), fibrotic breast tissue (FBT), and tumoral breast tissue (TBT) stiffness. Cell viability was assessed using an MTT assay at 1, 3, and 7 days. Absorbance was measured at 570 nm with a reference wavelength of 630 nm (n = 4). (b) Stemness gene expression. Relative mRNA expression of stemness-related genes *Sox2*, *Nanog*, and *Oct4* in 4T1 cells cultured on NBT, FBT, and TBT scaffolds for 7 days. Gene expression was determined by quantitative real-time PCR and normalized to NBT levels (n = 3). Data are expressed as mean ± SD. Statistical significance is indicated as follows: *$p < 0.05$, **$p < 0.01$, ***$p < 0.001$, and ****$p < 0.0001$.

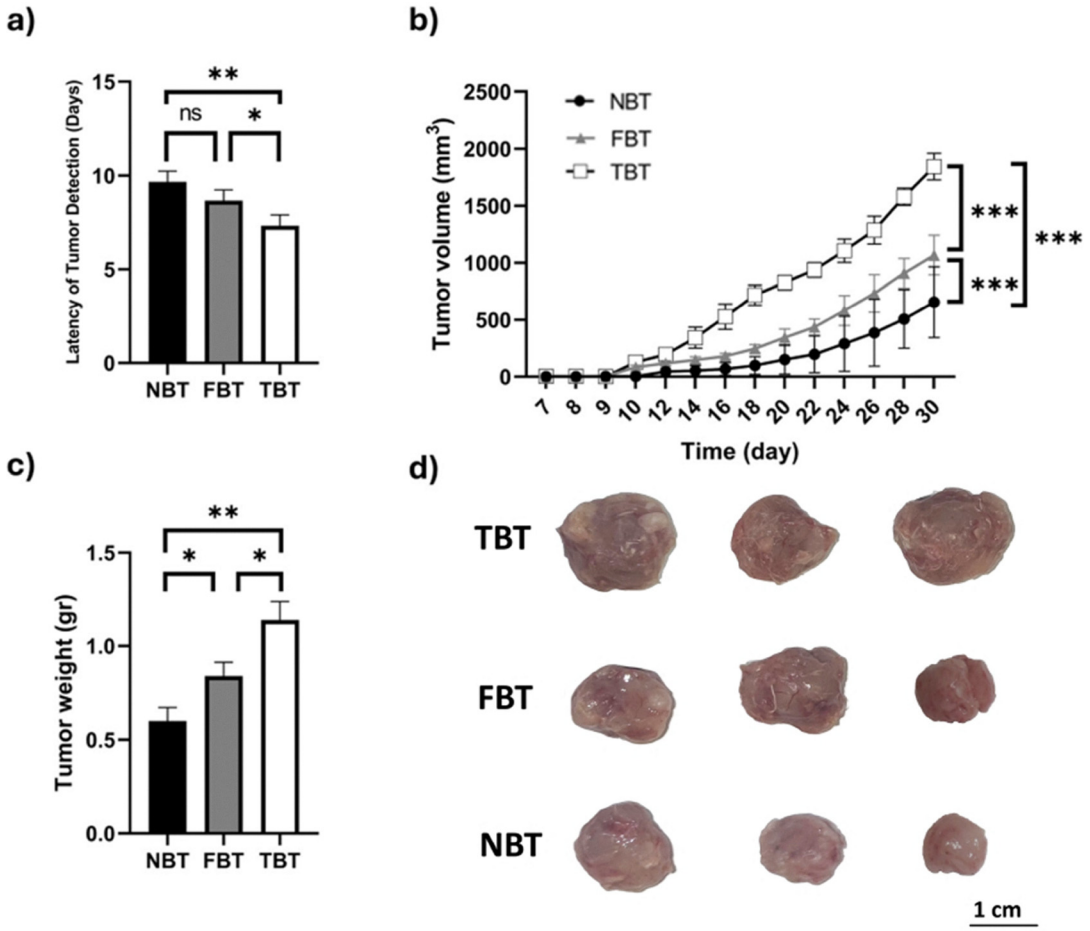

Fig. 4 Impact of scaffold stiffness pre-conditioning on 4T1 tumor progression *in vivo*. 4T1 murine mammary carcinoma cells were cultured on chitosan–alginate scaffolds mimicking normal breast tissue (NBT), fibrotic breast tissue (FBT), or tumoral breast tissue (TBT) stiffness before orthotopic implantation into mice. (a) Tumor latency (days to palpable tumor formation) following implantation of 4T1 cells pre-cultured on NBT, FBT, or TBT scaffolds. (b) Tumor growth curves showing tumor volume (mm^3) over time (days post-implantation) for 4T1 cells pre-cultured on NBT, FBT, or TBT scaffolds. (c) Final tumor weight (g) measured on day 30 post-implantation for each pre-conditioning group. (d) Representative photographs of tumors harvested on day 30 post-implantation from mice injected with 4T1 cells pre-cultured on NBT, FBT, or TBT scaffolds. Data are expressed as mean ± SD. Statistical significance is indicated as follows: $*p < 0.05$, $**p < 0.01$, $***p < 0.001$, and $****p < 0.0001$.

Fig. 4, tumor latency analysis revealed a significant reduction in latency in TBT mice compared to the other groups following the injection of detached 4T1 cells. Moreover, a significant increase in tumor volume and weight in the TBT group compared to the NBT and FBT groups was detected. Additionally, there was a statistically significant reduction in tumor volume and weight in the NBT group compared to the FBT group. While the sample size limits broad statistical generalization, the consistent and substantial magnitude of these differences (including an approximate 200% increase in the primary tumor volume in the TBT group compared to the NBT group) indicates a strong biological effect of stiffness preconditioning on tumorigenic potential.

3.10 Metastatic potential of 4T1 cells cultured on scaffolds with varying stiffness

3.10.1 Histological analysis of the lung and liver in 4T1 tumor-bearing mice. For histopathological evaluation, the primary tumor along with the lung and liver were examined in NBT, FBT, and TBT mouse groups (Fig. 5). MI/HPF was higher in the TBT[33] group compared to NBT[22] and FBT.[13] That suggests that tumor cells, which were pre-cultured on stiffer scaffold, TBT, were more proliferative and aggressive, consistent with increased tumor volume and weight observed in this group. In tumor of NBT groups, there isn't any necrotic tissue, but FBT groups showed small foci of necrosis and in TBT groups, there is multiple severe necrotic tissue were detected. Also, in control group, no pathological alterations were detected in all examined tissues. In the NBT group, the lungs exhibited small metastatic lesions composed of tumor cells with hyperchromatic nuclei and scant cytoplasm. Additionally, type 2 pneumocyte hyperplasia was observed along the alveolar walls. The FBT group displayed small metastatic nodules in the lungs, along with tumor cell proliferation and embolization within the interlobular spaces. Increased inflammatory cell infiltration was also noted in the alveolar walls. In the TBT

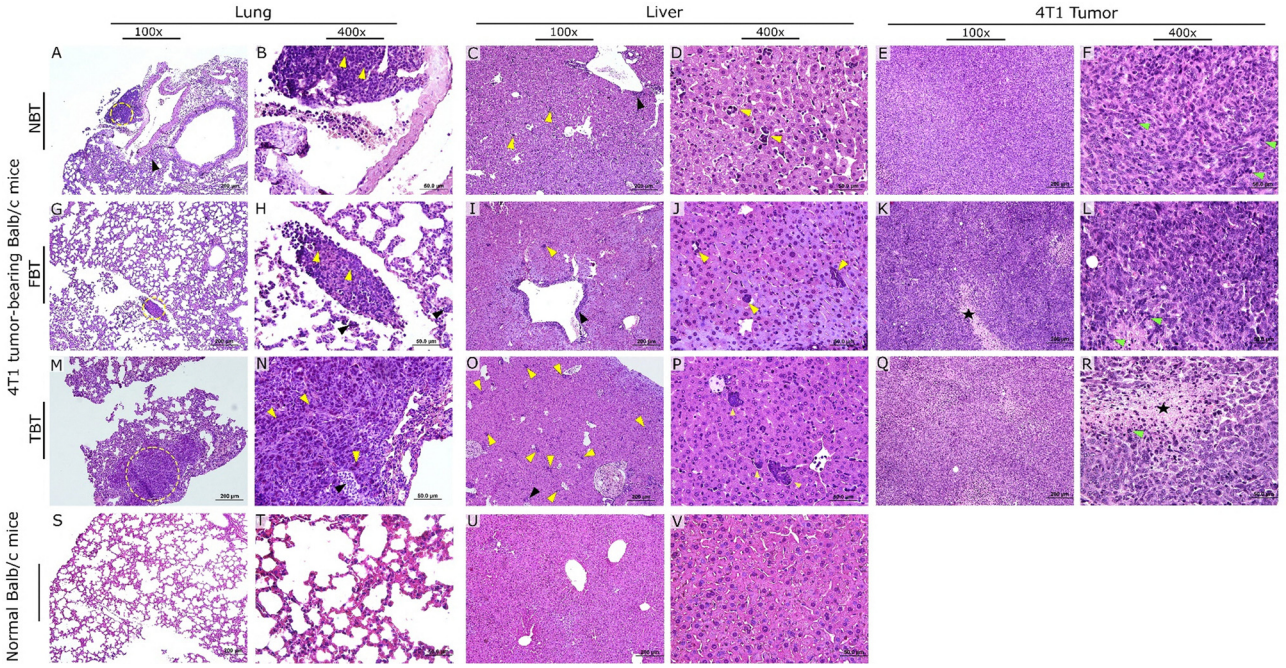

Fig. 5 Histopathological analysis of primary tumors and metastases. Representative hematoxylin and eosin (H&E) stained images of lung, liver, and primary tumor tissues from mice injected with 4T1 cells pre-cultured on scaffolds mimicking the stiffness of normal (NBT), fibrotic (FBT), and tumoral (TBT) mouse breast tissues, and from control mice. Lung tissue: NBT (A, B), FBT (G, H), TBT (M, N), Control (S, T). Liver tissue: NBT (C, D), FBT (I, J), TBT (O, P), Control (U, V). Primary tumor tissue: NBT (E, F), FBT (K, L), TBT (Q, R). Yellow arrowheads indicate metastatic cancer cells, black arrowheads indicate interstitial granulocyte infiltration, yellow circles indicate metastatic foci, green arrowheads indicate proliferating cells, and black stars indicate necrotic centers. Scale bars: 100× magnification = 200 μm; 400× magnification = 50 μm.

group, large metastatic nodules in lung sections were seen. Diffuse and intense inflammatory infiltration was observed in the alveolar walls both near and within the metastatic foci. Comparative analysis revealed that the TBT group had significantly larger pulmonary metastatic nodules, a higher mitotic index, and greater inflammatory cell infiltration compared to the NBT and FBT groups.

In the liver of the NBT group, small metastatic foci of 4T1 cancer cells (localized clusters of tumor cells) were detected, along with inflammatory cell infiltration in the portal spaces. In the FBT group, metastatic foci were detected in the liver parenchyma, and inflammatory cells were infiltrated into the central vein wall. In the TBT group, numerous hepatic metastatic foci were observed in liver parenchyma. Multiple mononuclear inflammatory cells infiltration was detected in portal spaces. Microscopic analysis between the liver of NBT, FBT, and TBT groups showed that the numbers of liver metastatic foci were significantly increased in TBT groups.

Quantification analysis of H&E-stained slides revealed that the mean number of lung metastases nodules in the NBT, FBT, and TBT mice groups was 0.5, 0.7, and 0.9, respectively. In addition, the lung metastatic nodules in the TBT group were larger than those in the other two groups. The mean number of liver metastatic nodules was quantified as 7.6, 8.9, and 15.4 for the NBT, FBT, and TBT groups, respectively (Fig. 6(a) and (b)). A semiquantitative analysis was conducted on lung and liver tissue sections from 4T1 tumor-bearing mice to estimate the average percentage of parenchymal area occupied by metastases foci using ImageJ software (Fig. 6(c) and (d)). The mean percentage of lung parenchyma occupied by metastases was 1.9, 3.4 and 6.7 in the NBT, FBT, and TBT groups, respectively. Furthermore, the average percentage of metastases area in the liver was 1.6%, 1.9%, and 3.7% in the NBT, FBT, and TBT mouse groups, respectively. (Fig. 6(c) and (d)). The results demonstrated that TBT group exhibited a significantly larger metastatic area compared to other groups.

3.10.2 *Plac1* expression in the lung and liver of 4T1 breast cancer model. While 4T1 cancer cells express *Plac1*, normal lung and liver cells (both metastatic targets of breast cancer) do not. Therefore, real-time PCR was conducted to determine cancer cell burden by measuring *Plac1* expression in the lungs and liver of mice with breast cancer. The mRNA expression of *Plac1* was compared in the liver and lungs of mice injected with cells primed on NBT, FBT, and TBT scaffolds. The TBT group showed a significant increase in *Plac1* expression in both the liver and lungs compared to the NBT and FBT groups. Furthermore, while the FBT group also exhibited higher *Plac1* expression in the liver and lungs compared to the NBT group, this increase was not statistically significant (Fig. 7).

The order-of-magnitude increase in *Plac1* expression in the TBT group, alongside the histopathological evidence, provides compelling evidence that preconditioning on a stiff, tumor-mimicking matrix imprints a persistent mechanical memory that potently enhances the metastatic potential of 4T1 cells.

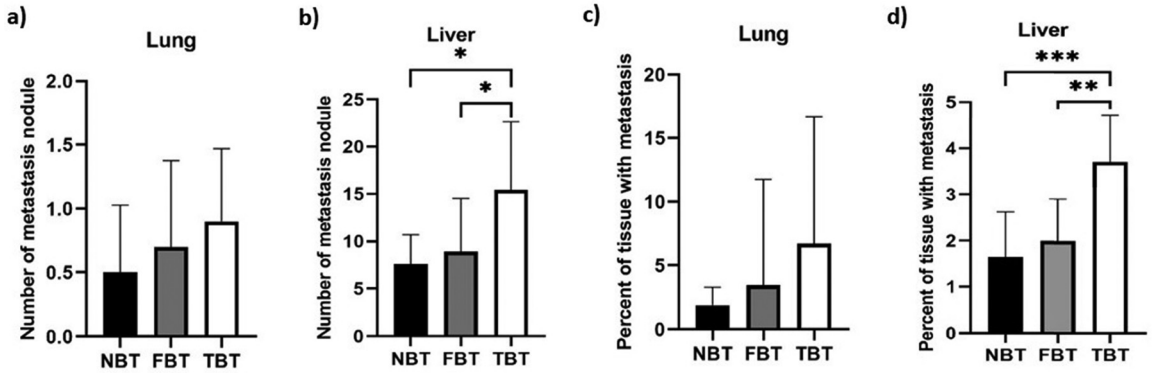

Fig. 6 Quantification of metastasis in the lung and liver of NBT, FBT and TBT mice groups. The mean number of metastatic nodules was calculated per histologic section in the (a) lung and (b) liver of NBT, FBT and TBT mice groups. The mean percentage of tissue parenchyma with metastases was quantified in the (c) lung and (d) liver of NBT, FBT and TBT mice groups. A software-based analysis was performed to calculate the percentage of tissue parenchyma involved by metastasis across all relevant fields. Statistical significance is indicated as follows: *$p < 0.05$, **$p < 0.01$, and ***$p < 0.001$.

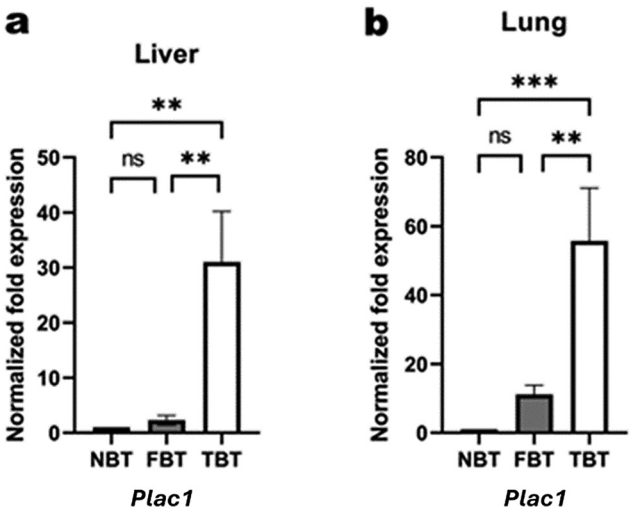

Fig. 7 *Plac1* expression in metastatic organs. Relative *Plac1* mRNA expression in (a) liver and (b) lungs of mice bearing 4T1 breast tumors. 4T1 cells were pre-cultured on scaffolds mimicking normal (NBT), fibrotic (FBT), or tumoral (TBT) breast tissue stiffness before orthotopic injection. Gene expression was measured by qRT-PCR and normalized to NBT levels. Data are expressed as mean ± SD ($n = 3$). Statistical significance is indicated as follows: *$p < 0.05$, **$p < 0.01$, ***$p < 0.001$, and ****$p < 0.0001$.

4. Discussion

The TME, particularly the ECM, significantly influences tumor growth, metastasis, and tumor cell behavior.[13] Indeed, a rigid ECM contributes to all cancer hallmarks, including proliferation, growth, immortality, death resistance, angiogenesis, invasion, avoidance of immune destruction, and drug resistance.[13,35] This study investigated the impact of matrix stiffness, mimicking normal, fibrotic, and tumoral breast tissue, on 4T1 murine breast cancer cell characteristics and metastatic potential using chitosan–alginate scaffolds to discriminate stiffness effects from biochemical confounders present in other matrixes like collagen gels. Moving beyond the established link between matrix stiffness, stemness, and metastasis, this study offers a holistic, *in vivo* investigation into sustained mechanical memory, a critical advancement for the field. This work makes a unique contribution through an integrated experimental framework designed to meticulously trace the influence of a transient mechanical cue on metastases burden. Using an orthotopic tumor model, which closely mimics natural breast cancer progression, we demonstrated that this mechanical memory not only drives accelerated primary tumor progression but, crucially, also promotes spontaneous metastasis to the lungs and liver. This provides direct evidence that a mechanical signal from a primary environment can confer a persistent, pro-metastatic phenotype, influencing the cancer cell's long-term success to initiate, progress, and disseminate the disease. Thus, our work serves as a critical bridge between controlled *in vitro* mechanobiology and complex *in vivo* tumorigenesis, offering a novel perspective on how biomechanical priming predetermines metastatic outcomes. To simulate the biomechanical properties of breast tissues across a range of pathological states, we engineered alginate–chitosan scaffolds with stiffnesses mimicking normal, fibrotic, and tumoral states. As is characteristic of polymer hydrogels, increasing the polymer concentration to achieve higher stiffness resulted in correlated changes in physical properties, including reduced average pore size, lower porosity, and decreased swelling capacity.[36,37] This interdependence mirrors the *in vivo* scenario, where pathological ECM remodeling during fibrosis and cancer progression concurrently increases stiffness, reduces pore size, and alters hydraulic conductivity.[38,39] For example, collagen densification in tumors increases mechanical resistance while reducing interstitial space and hindering fluid flow.[40] Although these properties are linked in our system, all scaffolds maintained a porous, interconnected architecture conducive to 3D cell culture, supporting cell infiltration, proliferation, and nutrient/waste exchange. The observed biological outcomes are likely a result of this combined biophysical cue set, which collectively mimics a pro-tumorigenic microenvironment. This highlights that the malignant progression driven by the TME is

not governed by stiffness alone but by a symphony of mechanical and topological signals.[41,42] Our model provides a platform to study these coupled effects, which are representative of real tissue pathomechanics. Future work employing scaffolds with orthogonally tunable properties will be valuable to decouple the specific contributions of each parameter.

In detail, our *in vitro* experiments revealed a direct link between matrix stiffness, cell morphology, viability, and stemness. 4T1 cells cultured on TBT scaffolds exhibited stellate morphologies, formed spheroid-like aggregates with invasive features,[43] and showed significantly increased viability and stemness-related gene expression (*Sox2*, *Nanog*, *Oct4*), consistent with previous reports.[14,44–46] Conversely, cells on NBT scaffolds displayed round morphology, sheet-like aggregation, and lower viability and stemness marker expression. These *in vitro* observations provide a mechanistic link to our *in vivo* findings. We acknowledge that the MTT assay primarily quantifies metabolic activity, which can be significantly influenced by matrix stiffness independent of cell number, rather than being a direct measure of cell numbers alone. Furthermore, electron microscopy has been used to assess the morphology of cells cultured on scaffolds, though these observations may have been influenced by sample preparation artifacts. For a more accurate and quantitative evaluation of cell morphology, particularly in a 3D environment, future studies should employ methods such as confocal microscopy with staining of the cytoskeleton and nuclei. This approach provides high-resolution three-dimensional visualization of cell shape and spreading while facilitating robust quantitative morphological analysis, thereby overcoming the inherent limitations of SEM for such applications.

While our study provides a robust model for the role of mechanical memory in the aggressive TNBC-like 4T1 line, we acknowledge the mechanobiological response and the phenomenon of mechanical memory may vary significantly across different breast cancer subtypes (such as ER^+ or $HER2^+$) due to their distinct genetic drivers and signaling pathways.[47] Future research must validate these findings in other cell lines, including luminal and HER2-positive human models, and, ideally, in patient-derived organoids or xenografts to confirm the broad clinical relevance of stiffness-induced mechanical memory.

Our *in vivo* study demonstrated that 4T1 cells pre-conditioned on TBT scaffolds formed tumors with significantly more aggressive behavior compared to those pre-conditioned on NBT or FBT scaffolds, including reduced tumor latency, increased tumor volume and weight, and increased lung and liver metastasis. This highlights the profound and persistent influence of TME stiffness on breast cancer progression and metastasis, demonstrating mechanical memory. This mechanical memory may involve epigenetic modifications, such as DNA methylation and histone modifications, altering gene expression patterns in response to mechanical cues.[48] For instance, stiffness-induced changes in chromatin accessibility could lead to long-term alterations in the expression of genes involved in cell motility, stemness, and survival.[49]

The molecular mechanisms underpinning the observed mechanical memory and its persistent pro-metastatic effects are hypothesized to operate through a two-phase process. An initial mechanotransduction signal induces epigenetic modifications that stabilize cellular characteristics. We propose that the stiff alginate–chitosan microenvironment first triggers a canonical mechanosensing cascade,[50,51] wherein the activation of mechanosensitive ion channels (such as TRP and Piezo), integrins, and CD44 leads to FAK phosphorylation and activation of downstream effectors like SRC and PI3K/Akt.[52,53] This force-transduction inhibits the Hippo pathway, promoting nuclear localization of YAP/TAZ[54,55] and driving a transcriptional program for proliferation and stemness characteristics,[56] the phenotypes we observed. Crucially, we hypothesize that this initial YAP/TAZ-driven transcription is subsequently locked in by epigenetic modifications. Evidence suggests that sustained mechanical stimulation can induce lasting changes in chromatin accessibility, histone marks (such as H3K27ac and H3K4me3), and DNA methylation at promoters of mechanoresponsive genes.[57,58] This epigenetic reprogramming would provide a plausible molecular basis for the "mechanical memory", ensuring the maintenance of transcriptional state even after the cells detached from the primary stiff niche. While our data on stemness gene expression are consistent with this model, definitive confirmation through the epigenetic assays (such as ATAC-seq and ChIP-qPCR) remains an essential and logical next step to fully validate this proposed mechanism.

The current study, demonstrating that stiffness alone is sufficient to imprint a pro-metastatic mechanical memory in 4T1 murine breast cancer cells using biodegradable chitosan–alginate scaffolds mimicking normal, fibrotic, or tumoral breast tissue stiffness, aligns with a significant body of *in vivo* research highlighting the tumor-promoting effects of increased matrix stiffness. For instance, studies on $ER\alpha^+$ breast cancer in mice with collagen-dense mammary glands showed that increased collagen-I enhanced circulating tumor cells and pulmonary metastases without altering primary tumor growth.[59] In a model of bone metastasis, stiff-primed MDA-MB-231 cells led to higher rates of osteolytic lesions, suggesting that primary tumor mechanical conditioning influences metastatic behavior.[60] Beyond breast cancer, elevated matrix stiffness has been linked to liver metastasis of colorectal cancer, where tumor pericytes expressing Transcription Factor 21 (TCF21) increase perivascular ECM stiffness through collagen remodeling and promote metastatic dissemination from the primary tumor site.[61] Pancreatic cancer metastasis was strikingly exacerbated in fibrotic (stiff) livers with type-I collagen deposition, awakening dormant cancer cells.[62] In melanoma, genetically reducing matrix stiffness by depleting biglycan, an extracellular matrix proteoglycan, led to reduced tumor growth, metastasis, and increased integrin-β1 expression, further supporting stiffness as a promoter of invasion.[63] Neuroblastoma with a stiff ECM, rich in cross-linked collagen, was associated with an aggressive phenotype and genomic heterogeneity.[64] In non-small cell lung cancer (NSCLC), increased levels of CD248 in cancer-associated fibroblasts induced collagen I formation and enhanced ECM

stiffness, facilitating NSCLC cell infiltration and migration and metastasis, and stromal α11 expression linked to collagen cross-linking also promoted tumorigenicity and metastasis.[65] Moreover, in bladder cancer, reducing collagen I and III content through GABPA (GA-binding protein transcription factor alpha subunit) overexpression led to diminished metastasis, implicitly supporting that increased stiffness would promote it.[66]

However, the field also presents nuanced and sometimes contradictory findings. Notably, some *in vivo* breast cancer studies found an inverse correlation between tumor stiffness and metastatic potential; softer primary mammary tumors were associated with significantly more metastases and local recurrences than stiffer tumors.[67] One such study, also focusing on TNBC, reported that cancer cells exposed to softer microenvironments were more able to colonize secondary tissues in an experimental tail vein lung metastasis model, driven by enhanced fatty acid metabolism.[68] These discrepancies underscore the complexity of mechanobiology in cancer, potentially reflecting differences in cancer type, specific cell lines, the models used, the methods of stiffness assessment (correlating stiffness values across studies is challenging due to inconsistencies in measurement protocols), and the specific molecular mechanisms engaged in different tissue microenvironments and metastatic stages.[67] This ongoing debate emphasizes the need for further research to explore the effects of matrix stiffness on cancer progression in a context dependent manner.

While our study demonstrates that matrix stiffness alone can induce persistent mechanical memory, we acknowledge that our fibrotic breast tissue (FBT)-mimetic scaffold does not fully recapitulate the complexity of *in vivo* fibrotic microenvironments. Fibrosis in breast tissue involves not only increased stiffness but also compositional changes and topological alterations.[69,70] These factors collectively influence cellular signaling and disease progression.[71–73] For instance, aligned collagen fibers can promote directed migration and invasion, while altered ECM composition can activate integrin-mediated signaling pathways independently of stiffness.[70,73,74] Our scaffold system, by design, isolates stiffness from these confounders to pinpoint its specific role. However, the stiffness value for FBT was inferred from the literature rather than directly measured in murine fibrotic mammary tissue, which may vary based on the extent of collagen deposition and cross-linking. Future studies should directly characterize the mechanical properties of fibrotic mammary tissue in murine models and incorporate complementary biochemical and architectural cues into engineered scaffolds to more accurately model fibrosis-associated ECM.

This study has other limitations. Scaffold variability, while minimized by our standardized preparation, could still influence results. The 4T1 model, while useful, does not fully recapitulate the complexity of human breast cancer. Future studies should investigate other breast cancer subtypes, including ER^+ and $HER2^+$ models, and explore patient-derived xenografts for improved clinical relevance. Furthermore, investigating specific epigenetic modifications and cytoskeletal rearrangements involved in mechanical memory is warranted. Future studies should investigate how the duration of matrix preconditioning influences the longevity of mechanical memory and assess whether stiffness-induced phenotypic changes remain reversible or become irreversible upon re-exposure to varying microenvironmental stiffness conditions. Finally, future studies should investigate the potential of stiffness as a biomarker for patient stratification and therapeutic guidance, potentially through imaging techniques or biopsies.

Finally, while this study focused on replicating the elastic modulus of breast tissues, it is important to recognize that the native TME is fundamentally viscoelastic, exhibiting complex, time-dependent mechanical behaviors such as stress relaxation and creep. Emerging research underscores that these dynamic properties are not mere biological background but are active regulators of cell behavior and potent biomarkers of disease state. For instance, recent studies in liver fibrosis have demonstrated that viscoelastic multiscale mechanical indexes, particularly power-law rheology parameters, can discriminate between healthy, fibrotic, and treated tissues with greater sensitivity than static stiffness measurements alone.[75] Beyond being a biomarker, this viscoelasticity is a potent regulator of cell fate, influencing fundamental processes like cytoskeletal remodeling and stem cell lineage commitment.[76] In cancer, these multiscale viscoelastic features influence migration, proliferation, and stemness, suggesting cells may possess a distinct "viscoelastic memory" that operates beyond stiffness sensing alone.[77] Our scaffold system, which captures a key static mechanical cue, provides a foundational model for understanding stiffness-induced mechanical memory. Future work employing advanced biomaterials with independently tunable elastic and viscoelastic properties will be essential to disentangle the specific contributions of stress relaxation, energy dissipation, and other dynamic mechanical cues in the establishment and maintenance of a pro-metastatic mechanical memory. Such investigations will bridge the current gap between static *in vitro* models and the dynamically complex *in vivo* reality, ultimately leading to a more complete mechanobiological understanding of breast cancer progression.

5. Conclusion

This study demonstrates the persistence of stiffness-induced phenotypic changes (mechanical memory) in breast cancer cells, highlighting the critical role of matrix stiffness in promoting breast cancer progression and metastasis in a murine model. We show that tumor-mimicking stiffness induces morphological changes, enhances stemness, and drives aggressive tumor growth and metastasis. These effects are consistent with persistent mechanical memory mediated by, as we hypothesize, sustained mechanotransduction and epigenetic reprogramming. However, the specific molecular pathways and epigenetic modifications responsible require direct validation in future studies. Targeting mechanotransduction pathways, particularly proposed mediators like YAP/TAZ, may represent a promising therapeutic strategy, especially in aggressive subtypes like

TNBC. Future studies should focus on validating these mechanisms, developing and testing specific inhibitors in preclinical and clinical settings, exploring combination therapies, and investigating stiffness-related biomarkers for diagnostic and therapeutic purposes. These findings may also have implications for other solid tumors where matrix stiffness plays a significant role.

Abbreviation

Akt	Ak strain transforming
CAFs	Cancer-associated fibroblasts
CSCs	Cancer stem cells
DMSO	Dimethyl sulfoxide
ECM	Extracellular matrix
EMT	Epithelial–mesenchymal transition
ERK	Extracellular signal-regulated kinase
FAK	Focal adhesion kinase
FBS	Fetal bovine serum
FBT	Fibrotic breast tissue
FTIR	Fourier-transform infrared
H&E	Hematoxylin and Eosin
HPF	High power fields
HSP45	Heat shock protein 45
IBRC	Iranian biological resource center
KXA	Ketamine–xylazine–acepromazine cocktail
LOX	Lysyl oxidase
mTOR	Mechanistic target of rapamycin
MTT	3-(4,5-Dimethylthiazol-2-yl)-2,5-diphenyltetrazolium bromide
Nanog	Nanog Homeobox
NBT	Normal breast tissue
Oct4	Octamer-binding transcription factor 4
PI3K	Phosphoinositide 3-kinase
Plac1	Placenta-specific 1
SEM	Scanning electron microscopy
Sox2	SRY-Box transcription factor 2
TAZ	Transcriptional coactivator with PDZ-binding motif
TBT	Tumoral breast tissue
TGF-β	Transforming growth factor beta
3D	Three-dimensional
TME	Tumor microenvironment
TRP	Transient receptor potential
TNBC	Triple-negative breast cancer
wt%	Weight percent
YAP	Yes-associated protein

Ethics approval

The study was approved by the Ethics Committee of the Iran University of Medical Sciences (IR.IUMS.REC 1396.32781).

Author contributions

Sadegh Safaei: methodology, investigation, data curation, formal analysis, writing – original draft. Samane Heydari: writing – original draft, investigation, formal analysis. Masoumeh Dehghan Manshadi: investigation, formal analysis. Behnaz Ashtari: methodology. Mazaher Gholipourmalekabadi: methodology. Farhang Sasani: validation. Farideh Hashemi: investigation. Mehran Vosoogh: investigation. Zahra Madjd: supervision, validation, writing – review & editing. Roya Ghods: conceptualization, supervision, methodology, validation, writing – original draft, funding acquisition.

Conflicts of interest

The authors declare that they have no competing interests.

Data availability

All data will be shared by the corresponding author upon reasonable request.

Supplementary information (SI) is available. See DOI: https://doi.org/10.1039/d5ma00664c.

Acknowledgements

This work was supported by grants from the Iran University of Medical Sciences (no: 96-04-87-32781) and the Iran National Science Foundation (INSF) (no: 96015369). We are deeply grateful to Dr Hannaneh Golshahi for capturing the pathology photographs.

References

1 Z. Li, J. Li, X. Bai, X. Huang and Q. Wang, Tumor microenvironment as a complex milieu driving cancer progression: a mini review, *Clin. Transl. Oncol.*, 2024, 1–10.
2 K. Dzobo and C. Dandara, The Extracellular Matrix: Its Composition, Function, Remodeling, and Role in Tumorigenesis, *Biomaterials*, 2023, **8**(2), 146.
3 T. Oskarsson, Extracellular matrix components in breast cancer progression and metastasis, *Breast*, 2013, **22**, S66–S72.
4 M. W. Pickup, J. K. Mouw and V. M. Weaver, The extracellular matrix modulates the hallmarks of cancer, *EMBO Rep.*, 2014, **15**(12), 1243–1253.
5 S. M. Tarchi, M. Pernia Marin, M. M. Hossain and M. Salvatore, Breast stiffness, a risk factor for cancer and the role of radiology for diagnosis, *J. Transl. Med.*, 2023, **21**(1), 582.
6 L. Cassereau, I. Dean, Q. Shi, A. Au, C. Park, Y. Chen, J. Liphardt, E. Hwang and V. Weaver, Human breast cancer invasion and aggression correlates with ECM stiffening and immune cell infiltration, *Integr. Biol.*, 2015, **7**(10), 1120–1134.
7 A. Liman, B. Kabir, M. Abubakar, S. Abdullahi, S. Ahmed and S. Shehu, Triple-Negative Breast Cancer (TNBC) and its Luminal Androgen Receptor (LAR) subtype: A clinicopathologic

review of cases in a university hospital in Northwestern Nigeria, *Niger J. Clin. Pract.*, 2022, **25**(1), 97–104.

8 S. Ishihara and H. Haga, Matrix stiffness contributes to cancer progression by regulating transcription factors, *Cancers*, 2022, **14**(4), 1049.

9 M. Kalli, M. D. Poskus, T. Stylianopoulos and I. K. Zervantonakis, Beyond matrix stiffness: targeting force-induced cancer drug resistance, *Trends Cancer*, 2023, **9**(11), 937–954.

10 M. R. Atashzar, R. Baharlou, J. Karami, H. Abdollahi, R. Rezaei, F. Pourramezan and S. H. Zoljalali Moghaddam, Cancer stem cells: A review from origin to therapeutic implications, *J. Cell. Physiol.*, 2020, **235**(2), 790–803.

11 S. A. Mani, W. Guo, M. J. Liao, E. N. Eaton, A. Ayyanan, A. Y. Zhou, M. Brooks, F. Reinhard, C. C. Zhang, M. Shipitsin, L. L. Campbell, K. Polyak, C. Brisken, J. Yang and R. A. Weinberg, The epithelial-mesenchymal transition generates cells with properties of stem cells, *Cell*, 2008, **133**(4), 704–715.

12 T. B. Steinbichler, D. Savic, J. Dudás, I. Kvitsaridze, S. Skvortsov, H. Riechelmann and I. I. Skvortsova, Cancer stem cells and their unique role in metastatic spread, *Semin. Cancer Biol.*, 2020, **60**, 148–156.

13 S. Safaei, R. Sajed, A. Shariftabrizi, S. Dorafshan, L. Saeednejad Zanjani, M. Dehghan Manshadi, Z. Madjd and R. Ghods, Tumor matrix stiffness provides fertile soil for cancer stem cells, *Cancer Cell Int.*, 2023, **23**(1), 143.

14 L. Shah, A. Latif, K. J. Williams and A. Tirella, Role of stiffness and physico-chemical properties of tumour microenvironment on breast cancer cell stemness, *Acta Biomater.*, 2022, **152**, 273–289.

15 J. Sapudom, L. Kalbitzer, X. Wu, S. Martin, K. Kroy and T. Pompe, Fibril bending stiffness of 3D collagen matrices instructs spreading and clustering of invasive and non-invasive breast cancer cells, *Biomaterials*, 2019, **193**, 47–57.

16 L. Shah, A. Latif, K. J. Williams, E. Mancuso and A. Tirella, Invasion and Secondary Site Colonization as a Function of In Vitro Primary Tumor Matrix Stiffness: Breast to Bone Metastasis, *Adv. Healthcare Mater.*, 2023, **12**(3), e2201898.

17 F. Lin, H. Zhang, J. Huang and C. Xiong, Substrate Stiffness Coupling TGF-β1 Modulates Migration and Traction Force of MDA-MB-231 Human Breast Cancer Cells in Vitro, *ACS Biomater. Sci. Eng.*, 2018, **4**(4), 1337–1345.

18 A. J. Berger, K. M. Linsmeier, P. K. Kreeger and K. S. Masters, Decoupling the effects of stiffness and fiber density on cellular behaviors *via* an interpenetrating network of gelatin-methacrylate and collagen, *Biomaterials*, 2017, **141**, 125–135.

19 A. J. Berger, C. M. Renner, I. Hale, X. Yang, S. M. Ponik, P. S. Weisman, K. S. Masters and P. K. Kreeger, Scaffold stiffness influences breast cancer cell invasion *via* EGFR-linked Mena upregulation and matrix remodeling, *Matrix Biol.*, 2020, **85–86**, 80–93.

20 E. Cambria, M. F. Coughlin, M. A. Floryan, G. S. Offeddu, S. E. Shelton and R. D. Kamm, Linking cell mechanical memory and cancer metastasis, *Nat. Rev. Cancer*, 2024, **24**(3), 216–228.

21 S. Nemec and K. A. Kilian, Materials control of the epigenetics underlying cell plasticity, *Nat. Rev. Mater.*, 2021, **6**(1), 69–83.

22 L. W. Dunne, Z. Huang, W. Meng, X. Fan, N. Zhang, Q. Zhang and Z. An, Human decellularized adipose tissue scaffold as a model for breast cancer cell growth and drug treatments, *Biomaterials*, 2014, **35**(18), 4940–4949.

23 M. J. Paszek, N. Zahir, K. R. Johnson, J. N. Lakins, G. I. Rozenberg, A. Gefen, C. A. Reinhart-King, S. S. Margulies, M. Dembo, D. Boettiger, D. A. Hammer and V. M. Weaver, Tensional homeostasis and the malignant phenotype, *Cancer Cell*, 2005, **8**(3), 241–254.

24 S. J. Florczyk, F. M. Kievit, K. Wang, A. E. Erickson, R. G. Ellenbogen and M. Zhang, 3D Porous Chitosan-Alginate Scaffolds Promote Proliferation and Enrichment of Cancer Stem-Like Cells, *J. Mater. Chem. B*, 2016, **4**(38), 6326–6334.

25 A. Moeinzadeh, B. Ashtari, H. Garcia, M. Koruji, C. A. Velazquez, Z. Bagher, M. Barati, R. Shabani and S. M. Davachi, The Effect of Chitosan/Alginate/Graphene Oxide Nanocomposites on Proliferation of Mouse Spermatogonial Stem Cells, *J. Funct. Biomater.*, 2023, **14**(12), 556.

26 R. Sajed, A. H. Zarnani, Z. Madjd, S. Arefi, M. R. Bolouri, S. Vafaei, A. Samadikuchaksaraei, M. Gholipourmalekabadi, N. Haghighipour and R. Ghods, Introduction of an efficient method for placenta decellularization with high potential to preserve ultrastructure and support cell attachment, *Artif. Organs*, 2022, **46**(3), 375–386.

27 S. Saeedi Garakani, M. Khanmohammadi, Z. Atoufi, S. K. Kamrava, M. Setayeshmehr, R. Alizadeh, F. Faghihi, Z. Bagher, S. M. Davachi and A. Abbaspourrad, Fabrication of chitosan/agarose scaffolds containing extracellular matrix for tissue engineering applications, *Int. J. Biol. Macromol.*, 2020, **143**, 533–545.

28 H. Kang, Statistical messages from ARRIVE 2.0 guidelines, *Korean J. Pain*, 2021, **34**(1), 1–3.

29 A. Volarevic, B. Ljujic, V. Volarevic, M. Milovanovic, T. Kanjevac, A. Lukic and N. Arsenijevic, A new semiquantitative method for evaluation of metastasis progression, *J. Buon*, 2012, **17**(3), 585–590.

30 D. Sikpa, J. P. Fouquet, R. Lebel, P. Diamandis, M. Richer and M. Lepage, Automated detection and quantification of breast cancer brain metastases in an animal model using democratized machine learning tools, *Sci. Rep.*, 2019, **9**(1), 17333.

31 J. Mahmoudian, R. Ghods, M. Nazari, M. Jeddi-Tehrani, M. H. Ghahremani, S. N. Ostad and A. H. Zarnani, Expression profiling of plac1 in murine cancer cell lines, *Exp. Oncol.*, 2019, **41**(1), 7–13.

32 S. Safaei, M. Dehghan Manshadi, H. Golshahi, F. Hashemi, F. Sasani, Z. Madjd and R. Ghods, Placenta specific 1: a novel marker for detection of metastasis in mouse model of breast cancer, *Biomarkers*, 2025, 1–13.

33 J. Mahmoudian, R. Ghods, M. Nazari, M. Jeddi-Tehrani, M. H. Ghahremani, N. Ghaffari-Tabrizi-Wizsy, S. N. Ostad and A. H. Zarnani, PLAC1: biology and potential application in cancer immunotherapy, *Cancer Immunol. Immunother.*, 2019, **68**(7), 1039–1058.

34 E. C. Filipe, S. Velayuthar, A. Philp, M. Nobis, S. L. Latham, A. L. Parker, K. J. Murphy, K. Wyllie, G. S. Major, O. Contreras, E. T. Y. Mok, R. F. Enriquez, S. McGowan, K. Feher, L. E. Quek, S. E. Hancock, M. Yam, E. Tran, Y. F. I. Setargew, J. N. Skhinas, J. L. Chitty, M. Phimmachanh, J. Z. R. Han, A. L. Cadell, M. Papanicolaou, H. Mahmodi, B. Kiedik, S. Junankar, S. E. Ross, N. Lam, R. Coulson, J. Yang, A. Zaratzian, A. M. Da Silva, M. Tayao, I. L. Chin, A. Cazet, M. Kansara, D. Segara, A. Parker, A. J. Hoy, R. P. Harvey, O. Bogdanovic, P. Timpson, D. R. Croucher, E. Lim, A. Swarbrick, J. Holst, N. Turner, Y. S. Choi, I. V. Kabakova, A. Philp and T. R. Cox, Tumor Biomechanics Alters Metastatic Dissemination of Triple Negative Breast Cancer *via* Rewiring Fatty Acid Metabolism, *Adv. Sci.*, 2024, **11**(23), e2307963.

35 M. W. Pickup, J. K. Mouw and V. M. Weaver, The extracellular matrix modulates the hallmarks of cancer, *EMBO Rep.*, 2014, **15**(12), 1243–1253.

36 C. M. Madl and S. C. Heilshorn, Engineering Hydrogel Microenvironments to Recapitulate the Stem Cell Niche, *Annu. Rev. Biomed. Eng.*, 2018, **20**, 21–47.

37 S. R. Caliari and J. A. Burdick, A practical guide to hydrogels for cell culture, *Nat. Methods*, 2016, **13**(5), 405–414.

38 P. P. Provenzano, D. R. Inman, K. W. Eliceiri, J. G. Knittel, L. Yan, C. T. Rueden, J. G. White and P. J. Keely, Collagen density promotes mammary tumor initiation and progression, *BMC Med.*, 2008, **6**, 11.

39 S. Kumar and V. M. Weaver, Mechanics, malignancy, and metastasis: the force journey of a tumor cell, *Cancer Metastasis Rev.*, 2009, **28**(1–2), 113–127.

40 T. Stylianopoulos, J. D. Martin, V. P. Chauhan, S. R. Jain, B. Diop-Frimpong, N. Bardeesy, B. L. Smith, C. R. Ferrone, F. J. Hornicek, Y. Boucher, L. L. Munn and R. K. Jain, Causes, consequences, and remedies for growth-induced solid stress in murine and human tumors, *Proc. Natl. Acad. Sci. U. S. A.*, 2012, **109**(38), 15101–15108.

41 O. Chaudhuri, J. Cooper-White, P. A. Janmey, D. J. Mooney and V. B. Shenoy, Effects of extracellular matrix viscoelasticity on cellular behaviour, *Nature*, 2020, **584**(7822), 535–546.

42 A. Buxboim, I. L. Ivanovska and D. E. Discher, Matrix elasticity, cytoskeletal forces and physics of the nucleus: how deeply do cells 'feel' outside and in?, *J. Cell Sci.*, 2010, **123**(Pt 3), 297–308.

43 E. García, C. Ragazzini, X. Yu, E. Cuesta-García, J. Bernardino de la Serna, T. Zech, D. Sarrió, L. M. Machesky and I. M. Antón, WIP and WICH/WIRE co-ordinately control invadopodium formation and maturation in human breast cancer cell invasion, *Sci. Rep.*, 2016, **6**, 23590.

44 U. L. Triantafillu, S. Park, N. L. Klaassen, A. D. Raddatz and Y. Kim, Fluid shear stress induces cancer stem cell-like phenotype in MCF7 breast cancer cell line without inducing epithelial to mesenchymal transition, *Int. J. Oncol.*, 2017, **50**(3), 993–1001.

45 G. M. Balachander, S. A. Balaji, A. Rangarajan and K. Chatterjee, Enhanced Metastatic Potential in a 3D Tissue Scaffold toward a Comprehensive in Vitro Model for Breast Cancer Metastasis, *ACS Appl. Mater. Interfaces*, 2015, **7**(50), 27810–27822.

46 M. F. Pang, M. J. Siedlik, S. Han, M. Stallings-Mann, D. C. Radisky and C. M. Nelson, Tissue Stiffness and Hypoxia Modulate the Integrin-Linked Kinase ILK to Control Breast Cancer Stem-like Cells, *Cancer Res.*, 2016, **76**(18), 5277–5287.

47 J. J. Northey, L. Przybyla and V. M. Weaver, Tissue Force Programs Cell Fate and Tumor Aggression, *Cancer Discovery*, 2017, **7**(11), 1224–1237.

48 R. Halder, M. Hennion, R. O. Vidal, O. Shomroni, R.-U. Rahman, A. Rajput, T. P. Centeno, F. Van Bebber, V. Capece and J. C. G. Vizcaino, DNA methylation changes in plasticity genes accompany the formation and maintenance of memory, *Nat. Neurosci.*, 2016, **19**(1), 102–110.

49 R. S. Stowers, A. Shcherbina, J. Israeli, J. J. Gruber, J. Chang, S. Nam, A. Rabiee, M. N. Teruel, M. P. Snyder and A. Kundaje, Matrix stiffness induces a tumorigenic phenotype in mammary epithelium through changes in chromatin accessibility, *Nat. Biomed. Eng.*, 2019, **3**(12), 1009–1019.

50 B. C. H. Cheung, X. Chen, H. J. Davis, C. S. Nordmann, J. Toth, L. Hodgson, J. E. Segall, V. B. Shenoy and M. Wu, Identification of CD44 as a key engager to hyaluronic acid-rich extracellular matrices for cell traction force generation and tumor invasion in 3D, *Matrix Biol.*, 2024, **135**, 1–11.

51 M. A. Schwartz, Integrins and extracellular matrix in mechanotransduction, *Cold Spring Harbor Perspect. Biol.*, 2010, **2**(12), a005066.

52 Y. Kim and S. Kumar, CD44-mediated adhesion to hyaluronic acid contributes to mechanosensing and invasive motility, *Mol. Cancer Res.*, 2014, **12**(10), 1416–1429.

53 X. Chen, S. Wanggou, A. Bodalia, M. Zhu, W. Dong, J. J. Fan, W. C. Yin, H. K. Min, M. Hu, D. Draghici, W. Dou, F. Li, F. J. Coutinho, H. Whetstone, M. M. Kushida, P. B. Dirks, Y. Song, C. C. Hui, Y. Sun, L. Y. Wang, X. Li and X. Huang, A Feedforward Mechanism Mediated by Mechanosensitive Ion Channel PIEZO1 and Tissue Mechanics Promotes Glioma Aggression, *Neuron*, 2018, **100**(4), 799–815.

54 S. Nasrollahi, C. Walter, A. J. Loza, G. V. Schimizzi, G. D. Longmore and A. Pathak, Past matrix stiffness primes epithelial cells and regulates their future collective migration through a mechanical memory, *Biomaterials*, 2017, **146**, 146–155.

55 C. Yang, M. W. Tibbitt, L. Basta and K. S. Anseth, Mechanical memory and dosing influence stem cell fate, *Nat. Mater.*, 2014, **13**(6), 645–652.

56 F. Zanconato, M. Cordenonsi and S. Piccolo, YAP/TAZ at the Roots of Cancer, *Cancer Cell*, 2016, **29**(6), 783–803.

57 F. M. Kievit, K. Wang, A. E. Erickson, S. K. Lan Levengood, R. G. Ellenbogen and M. Zhang, Modeling the tumor microenvironment using chitosan-alginate scaffolds to control the stem-like state of glioblastoma cells, *Biomater. Sci.*, 2016, **4**(4), 610–613.

58 C. Wang, X. Zhu, W. Feng, Y. Yu, K. Jeong, W. Guo, Y. Lu and G. B. Mills, Verteporfin inhibits YAP function through up-regulating 14-3-3σ sequestering YAP in the cytoplasm, *Am. J. Cancer Res.*, 2016, **6**(1), 27–37.

59 C. E. Barcus, K. A. O'Leary, J. L. Brockman, D. E. Rugowski, Y. Liu, N. Garcia, M. Yu, P. J. Keely, K. W. Eliceiri and L. A. Schuler, Elevated collagen-I augments tumor progressive signals, intravasation and metastasis of prolactin-induced estrogen receptor alpha positive mammary tumor cells, *Breast Cancer Res.*, 2017, **19**(1), 9.

60 A. W. Watson, A. D. Grant, S. S. Parker, S. Hill, M. B. Whalen, J. Chakrabarti, M. W. Harman, M. R. Roman, B. L. Forte, C. C. Gowan, R. Castro-Portuguez, L. K. Stolze, C. Franck, D. A. Cusanovich, Y. Zavros, M. Padi, C. E. Romanoski and G. Mouneimne, Breast tumor stiffness instructs bone metastasis *via* maintenance of mechanical conditioning, *Cell Rep.*, 2021, **35**(13), 109293.

61 X. Li, J. Pan, T. Liu, W. Yin, Q. Miao, Z. Zhao, Y. Gao, W. Zheng, H. Li, R. Deng, D. Huang, S. Qiu, Y. Zhang, Q. Qi, L. Deng, M. Huang, P. M. Tang, Y. Cao, M. Chen, W. Ye and D. Zhang, Novel TCF21(high) pericyte subpopulation promotes colorectal cancer metastasis by remodelling perivascular matrix, *Gut*, 2023, **72**(4), 710–721.

62 T. Zhang, J. Chen, H. Yang, X. Sun, Y. Ou, Q. Wang, M. Edderkaoui, S. Zheng, F. Ren, Y. Tong, R. Hu, J. Liu, Y. Gao, S. J. Pandol, Y. P. Han and X. Zheng, Stromal softness confines pancreatic cancer growth through lysosomal-cathepsin mediated YAP1 degradation, *Cell. Mol. Life Sci.*, 2024, **81**(1), 442.

63 H. Andrlová, J. Mastroianni, J. Madl, J. S. Kern, W. Melchinger, H. Dierbach, F. Wernet, M. Follo, K. Technau-Hafsi, C. Has, V. Rao Mittapalli, M. Idzko, R. Herr, T. Brummer, H. Ungefroren, H. Busch, M. Boerries, A. Narr, G. Ihorst, C. Vennin, A. Schmitt-Graeff, S. Minguet, P. Timpson, J. Duyster, F. Meiss, W. Römer and R. Zeiser, Biglycan expression in the melanoma microenvironment promotes invasiveness *via* increased tissue stiffness inducing integrin-β1 expression, *Oncotarget*, 2017, **8**(26), 42901–42916.

64 A. López-Carrasco, S. Martín-Vañó, R. Burgos-Panadero, E. Monferrer, A. P. Berbegall, B. Fernández-Blanco, S. Navarro and R. Noguera, Impact of extracellular matrix stiffness on genomic heterogeneity in MYCN-amplified neuroblastoma cell line, *J. Exp. Clin. Cancer Res.*, 2020, **39**(1), 226.

65 R. Navab, D. Strumpf, C. To, E. Pasko, K. S. Kim, C. J. Park, J. Hai, J. Liu, J. Jonkman, M. Barczyk, B. Bandarchi, Y. H. Wang, K. Venkat, E. Ibrahimov, N. A. Pham, C. Ng, N. Radulovich, C. Q. Zhu, M. Pintilie, D. Wang, A. Lu, I. Jurisica, G. C. Walker, D. Gullberg and M. S. Tsao, Integrin α11β1 regulates cancer stromal stiffness and promotes tumorigenicity and metastasis in non-small cell lung cancer, *Oncogene*, 2016, **35**(15), 1899–1908.

66 M. Dai, X. Yuan, C. Sun, R. Han, M. Björkholm, F. Kong, S. Zhao and D. Xu, The ETS transcription factor GABPA inhibits bladder cancer aggressiveness by repressing extracellular matrix deposition and mechanotransduction signaling, *Cell Death Dis.*, 2025, **16**(1), 618.

67 J. Fenner, A. C. Stacer, F. Winterroth, T. D. Johnson, K. E. Luker and G. D. Luker, Macroscopic stiffness of breast tumors predicts metastasis, *Sci. Rep.*, 2014, **4**, 5512.

68 E. C. Filipe, S. Velayuthar, A. Philp, M. Nobis, S. L. Latham, A. L. Parker, K. J. Murphy, K. Wyllie, G. S. Major, O. Contreras, E. T. Y. Mok, R. F. Enriquez, S. McGowan, K. Feher, L. E. Quek, S. E. Hancock, M. Yam, E. Tran, Y. F. I. Setargew, J. N. Skhinas, J. L. Chitty, M. Phimmachanh, J. Z. R. Han, A. L. Cadell, M. Papanicolaou, H. Mahmodi, B. Kiedik, S. Junankar, S. E. Ross, N. Lam, R. Coulson, J. Yang, A. Zaratzian, A. M. Da Silva, M. Tayao, I. L. Chin, A. Cazet, M. Kansara, D. Segara, A. Parker, A. J. Hoy, R. P. Harvey, O. Bogdanovic, P. Timpson, D. R. Croucher, E. Lim, A. Swarbrick, J. Holst, N. Turner, Y. S. Choi, I. V. Kabakova, A. Philp and T. R. Cox, Tumor Biomechanics Alters Metastatic Dissemination of Triple Negative Breast Cancer *via* Rewiring Fatty Acid Metabolism, *Adv. Sci.*, 2024, **11**(23), e2307963.

69 A. E. Mayorca-Guiliani, D. J. Leeming, K. Henriksen, J. H. Mortensen, S. H. Nielsen, Q. M. Anstee, A. J. Sanyal, M. A. Karsdal and D. Schuppan, ECM formation and degradation during fibrosis, repair, and regeneration, *npj Metab. Health. Dis.*, 2025, **3**(1), 25.

70 T. N. Wight and S. Potter-Perigo, The extracellular matrix: an active or passive player in fibrosis?, *Am. J. Physiol.: Gastrointest. Liver Physiol.*, 2011, **301**(6), G950–G955.

71 B. K. Patel, K. Pepin, K. R. Brandt, G. L. Mazza, B. A. Pockaj, J. Chen, Y. Zhou, D. W. Northfelt, K. Anderson, J. M. Kling, C. M. Vachon, K. R. Swanson, M. Nikkhah and R. Ehman, Association of breast cancer risk, density, and stiffness: global tissue stiffness on breast MR elastography (MRE), *Breast Cancer Res. Treat.*, 2022, **194**(1), 79–89.

72 X. Zhao, J. Chen, H. Sun, Y. Zhang and D. Zou, New insights into fibrosis from the ECM degradation perspective: the macrophage-MMP–ECM interaction, *Cell Biosci.*, 2022, **12**(1), 117.

73 S. Heydari, F. Tajik, S. Safaei, F. Kamani, B. Karami, S. Dorafshan, Z. Madjd and R. Ghods, The association between tumor-stromal collagen features and the clinical outcomes of patients with breast cancer: a systematic review, *Breast Cancer Res.*, 2025, **27**(1), 69.

74 R. Aparicio-Yuste, M. Muenkel, A. G. Clark, M. J. Gómez-Benito, E. E. Bastounis and A. Stiff, Extracellular Matrix Favors the Mechanical Cell Competition that Leads to Extrusion of Bacterially-Infected Epithelial Cells, *Front. Cell Dev. Biol.*, 2022, **10**, 912318.

75 Z. Chang, L. Zhang, J. T. Hang, W. Liu and G. K. Xu, Viscoelastic Multiscale Mechanical Indexes for Assessing Liver Fibrosis and Treatment Outcomes, *Nano Lett.*, 2023, **23**(20), 9618–9625.

76 V. D. L. Putra, K. A. Kilian and M. L. Knothe Tate, Biomechanical, biophysical and biochemical modulators of cytoskeletal remodelling and emergent stem cell lineage commitment, *Commun. Biol.*, 2023, **6**(1), 75.

77 Z. Chang, L. Y. Li, Z. J. Shi, W. Liu and G. K. Xu, Beyond stiffness: Multiscale viscoelastic features as biomechanical markers for assessing cell types and states, *Biophys. J.*, 2024, **123**(13), 1869–1881.